Available online at www.sciencedirect.com

ScienceDirect

Energy Procedia 112 (2017) 83 – 91

Energy Procedia

Sustainable Solutions for Energy and Environment, EENVIRO 2016, 26-28 October 2016, Bucharest, Romania

A performance study of a horizontal-axis micro-turbine in a numerical wave flume

Mustafa Tutar[a,b,*] and M. Mendi[c]

[a]*Mondragon Goi Eskola Politeknikoa, Loramendi 4,Arrasate-Mondragon, 20500,Spain*
[b]*IKERBASQUE, Basque Foundation for Science, 48011,Bilbao,Spain*
[c]*University of Mersin, Ciftlikkoy,Mersin,33343,Turkey*

Abstract

Numerical studies of performance of a 3-bladed Savonius type horizontal-axis wave energy converter are presented. Numerical simulations based on a volume of fluid (VOF) method coupled with a finite volume method (FVM) approach are performed in a numerical wave flume (NWF) for specified values of flow physics and turbine blade geometry conditions. Once validated against experimental data, the numerical simulations are extended to investigate the overall performance of the turbine over a very large range of wave height, wave frequency, and the submergence level for the same water depth in the context of optimization of a design of a small scale Savonius rotor. From the numerical results obtained and validated against the experimental data it can be concluded that the flow characteristics are strongly dependent upon differing wave propagation conditions and energy conversion rate can be increased with a proper combination of selected wave height and frequency for the investigated parametric value range.

Peer-review under responsibility of the organizing committee of the international conference on Sustainable Solutions for Energy and Environment 2016

Keywords: Savonius rotor; wave energy; numerical wave flume (NWF); volume of fluid element (VOF); finite volume method (FVM); energy conversion

1. Introduction

Fundamental wave energy conversion devices are mainly classified in three groups depending on how they interact with the ocean waves. In the first group, the turbine-type oscillating water columns (OWC) are devices that

* Corresponding author. Tel.: +34-943-79-4700 ; fax: +34-943-79-1536 .
E-mail address: mtutar@mondragon.edu

Peer-review under responsibility of the organizing committee of the international conference on Sustainable Solutions for Energy and Environment 2016
doi:10.1016/j.egypro.2017.03.1066

involve creating a structure on the shoreline such that waves enter and leave a static chamber. In the second group, overtopping devices consist of a structure which collects incoming waves by creating a reservoir into which only high waves may crash. In the third group, surface devices which directly use the motion of the ocean surface. They generally include a floating surface that moves up and down due to the buoyancy force of waves.

There have been number of experimental and numerical studies conducted for energy conversion analysis and performance research on ocean wave- energy converter (OWEC) devices constructed and tested in form of scale models in an experimental wave flume [1-6] and/or numerical wave flume [7-9]. These studies mainly focus on parametric analysis of design of such devices for increase of their wave energy conversion efficiency for a range of wave height, length and period and physical/geometrical constraints in relation to the wave motion. Modern wave channel instrumentations with the imposition of wave making technologies, PIV measurement and computer vision techniques to study of water waves can provide an ideal working medium for different types of scale models of OWEC devices in experimental wave flumes [2-4].

The aim of the present study is to numerically explore the non-linear, two-dimensional, viscous, unsteady and turbulent wave flow behavior over a Savonius rotor in comparison with the present authors´ previous experimental study [5] to provide possible solutions/suggestions for increasing hydrodynamic energy conversion efficiency of such devices by considering different operating conditions. The numerical analysis of Savonius rotor performance at intermediate-to-shallow water depths is not available in the known literature, and this is also motivation for the present study.

2. Mathematical principles

2.1. Governing equations

The basic flow equations governing the present turbulent flow behavior around a rotating constructed Savonius rotor structure are continuity and momentum conservation equations, i.e. Reynolds averaged Navier-Stokes (RANS) equations and transport equations for turbulence quantities. These conservation equations written in non-linear differential form of tensor notation for incompressible, viscous fluid flow conditions can be summarized below. For the present study, a fixed orthogonal coordinate system with origin at the center of the rolling cylinder is used for differential form of these equations.

$$\frac{\partial \bar{u}_i}{\partial x_i} = 0 \tag{1}$$

$$\rho \frac{\partial \bar{u}_i}{\partial t} + \rho \bar{u}_j \frac{\partial \bar{u}_i}{\partial x_j} = -\frac{\partial \bar{P}}{\partial x_i} + \frac{\partial}{\partial x_j}\left(\mu \frac{\partial \bar{u}_i}{\partial x_j} - \rho \overline{u_i' u_j'} \right) + \rho g_i \tag{2}$$

where ρ is the fluid density, $\bar{u}_i$ is the time averaged velocity, x_i is the coordinate direction, u_i' is the deviation from the time averaged velocity, $\bar{P}$ is the time averaged pressure, g is gravity acceleration, μ is the dynamic viscosity of the fluid, $-\rho \overline{u_i' u_j'}$ is the Reynold's stress tensor which appears on the right hand side of the RANS equations as a result of time averaging to the Navier-Stokes equations. The temporal and spatial co-ordinates correspond to t and x_i, respectively.

In eddy viscosity based k-ε turbulence models the turbulence field is characterized in terms of two transport variables, kinetic energy and its dissipation rate related to the time averaging to enclose the RANS equation (2) above. In the present study, the proposed model is based on Re-Normalised Group theory and is referred to as the RNG k-ε turbulence model [10]. This model is similar in form to the standard turbulence model; however the RNG turbulence model differs from the standard model by the inclusion of an additional sink term in the turbulence dissipation equation to account for non-equilibrium strain rates and employs different values for the various model coefficients.

In the present study, the volume of fluid element (VOF) method, initially proposed by Hirt and Nichols [11] is used as an algebraic volume-tracking method, in which air-water interface is not tracked explicitly but implicitly

captured by partially filled cells, to capture air-water interface advancement because of relatively topological robustness compared with moving mesh methods. In this method, a single set of momentum equations is shared by the fluids and the volume fractions of each of the fluids in each computational cell are tracked through domain.

2.2. Numerical details

The two-dimensional (2-D) numerical wave flume (NWF) constructed as a representation of the experimental wave flume (EWF) used in the authors´ previous study [5] is illustrated in Fig. 1. The overall size of the NWF is 24 m (length) x 0.60 m (width) x 0.75 m (depth).

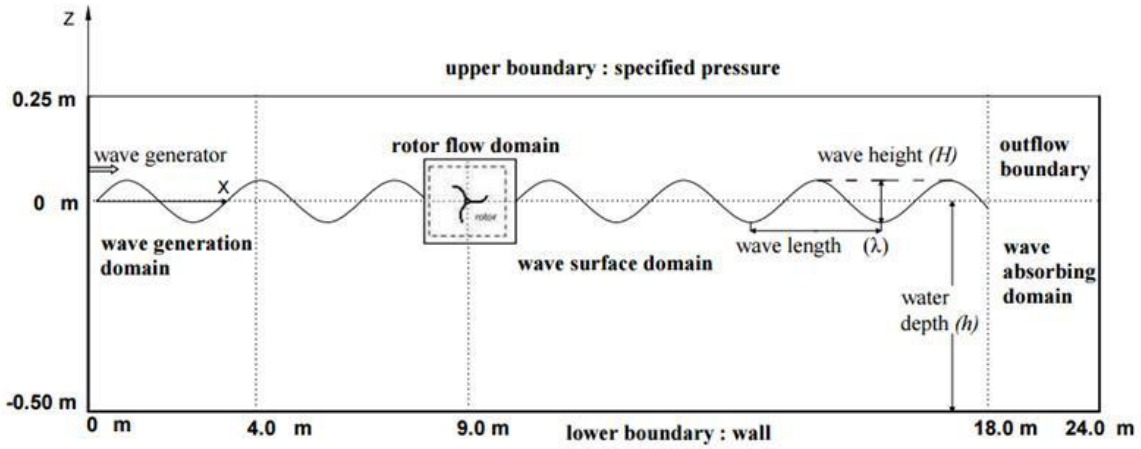

Fig. 1. The schematic of numerical wave flume (NWF) constructed as a representation of the experimental study [5]

The NWT is comprised of four different coupled sub-domains, namely, the wave generation domain, wave surface domain, rotor flow domain and wave absorbing domain as seen. The propagating waves are generated by a numerical wave generator at the left boundary of the NWT through the wave generation domain and the opening absorbing boundary is defined at the right-end boundary to prevent wave reflection back into the flow solution domain i.e. wave surface domain. The following below equations for the velocity components, u and w, in the x and z directions respectively are used for generating regular waves at the inflow boundary:

$$u=\frac{H}{2}\frac{gk}{\omega}\frac{\cosh k(h+z)}{\cosh kh}\cos(kx-\omega t)+\frac{3H^2\omega k}{16}\frac{\cosh 2k(h+z)}{\sinh^4(kh)}\cos 2(kx-\omega t) \tag{3}$$

$$w=\frac{H}{2}\frac{gk}{\omega}\frac{\sinh k(h+z)}{\cosh kh}\sin(kx-\omega t)+\frac{3H^2\omega k}{16}\frac{\sinh 2k(h+z)}{\sinh^4(kh)}\sin 2(kx-\omega t) \tag{4}$$

Where H is the wave height, ω is the wave frequency, k is the wave number, and h is the mean wave depth.

A finite difference method/finite volume method (FDM/FVM) based numerical flow modelling approach of FLOW-3D [12] is used to solve the three-dimensional (3-D), unsteady partial differential equations (continuity, momentum and energy equations) together with the turbulence transport equation, general motion (rotation) of the moving rotor body and the surface tracking. The momentum equations and the pressure based continuity equation are coupled with a pressure-velocity coupling scheme of Generalized Minimal Residual Solver (GMRES) scheme [13] and the second order upwind scheme for discretization of the momentum equation. Within this scheme,

pressure and velocity are coupled implicitly by using the time-advanced pressures in the momentum equations and the time advanced velocities in the continuity equations.

The geometric construction of rotor blades mounted on a 16.0 mm diameter rotor shaft with the same geometry profile of 59° bending blade angle and 2 mm thickness as studied experimentally is accomplished using a solid modelling CAD design software. Each blade has length of w = 480 mm and the rotor outer diameter of d = 252 mm which corresponds to about a diameter size of the orbital motion at the available highest wave height of 250 mm at submergence level of z = 0 mm. Figure 2 shows the generated solid geometry for the 3-bladed rotor structure.

Fig. 2. The 3-bladed Savonius rotor geometry constructed for the numerical simulations

A multi-block, nested, structured meshing system which enables higher mesh resolution in the rotor flow domain is utilized within the FLOW3D program [12]. The Fractional Area-Volume Obstacle Representation (FAVOR™), method, which defines the rotor geometry within the fixed (Eulerian) mesh by computing the fractional face areas (AF) and factional volume (VF) of rectangular structured mesh that are blocked by obstacles, is used. Figure 3 shows the generated multi-block mesh configuration containing optimum number of 111,800 mesh cells.

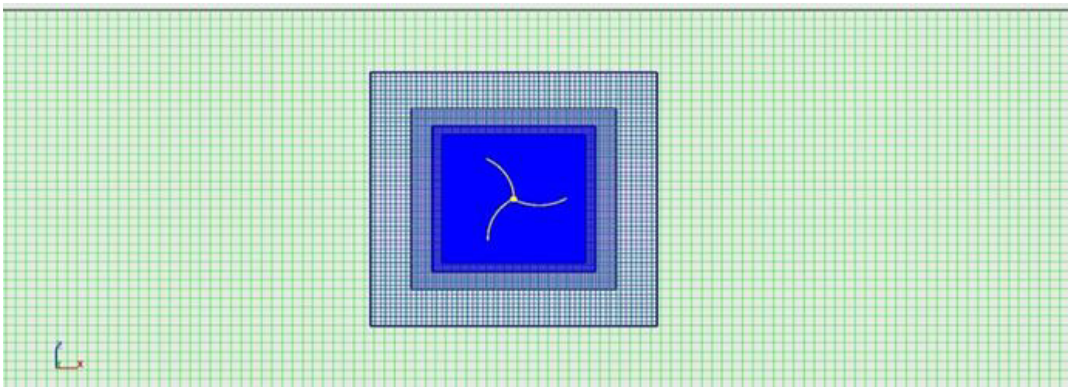

Fig. 3. The 5-nested-mesh blocks and corresponding rendered geometry of the rotor body for the medium mesh configuration

2.3. Numerical validation

A series of initial simulations are performed to evaluate the wave elevation in comparison with that of Stokes Second 2nd order wave theory to verify the present numerical approach for modelling of generation and propagation of regular (oscillatory) waves. Figure 4 clearly demonstrates the good correspondence between the numerical data retrieved at a probe position of P (9m, 0 m, -0.2 m) with the analytical theory for the selected medium mesh size of 111,800 mesh cells at a wave height of H = 100 mm and wave period of T = 1.5 s. The figure verifies the validity of the numerical approach to generate the regular waves based on the Stokes 2nd order theory.

3. Results and discussions

Following the numerical validation with the theoretical data for the no-rotor flow solution, simulations with the developed numerical modelling approach are extended to rotor-flow solution for three different wave heights of H = 100 mm, 150 mm, and 200 mm and wave periods of T = 1.5 s, 3.0 s, and 4.5 s at three different submergence positioning of z = -50 mm, 0 and +50 mm. Both qualitative and quantitative results are reproduced to make an extensive performance analysis of the NWF application by calculating rotational speed, torque values in accordance with the experimental data.

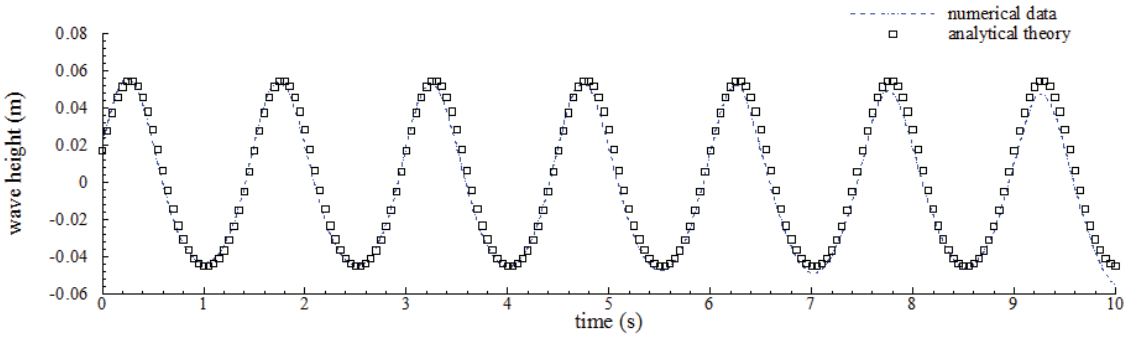

Fig. 4. Wave elevation history computed at a probe position of x = 9 m, y = 0 and z = -0.2 m at a wave height of H = 100 mm and wave period of T = 1.5 s for the optimum mesh configuration

The flow patterns around the rotor structure are observed qualitatively in images of instantaneous phase contours and velocity vectors at different operating conditions. Figures 5 illustrates the instantaneous phase contours together with velocity vector fields over a one-wave period (4th- wave cycle) at H = 100 mm, T = 1.5 s and z = 0 mm . The figure clearly identifies the backward and forward motion of the rotor i.e fluctuating rotor movement in the clockwise and –counterclockwise position with the interaction of the upcoming waves, upstream and downstream of the rotor.

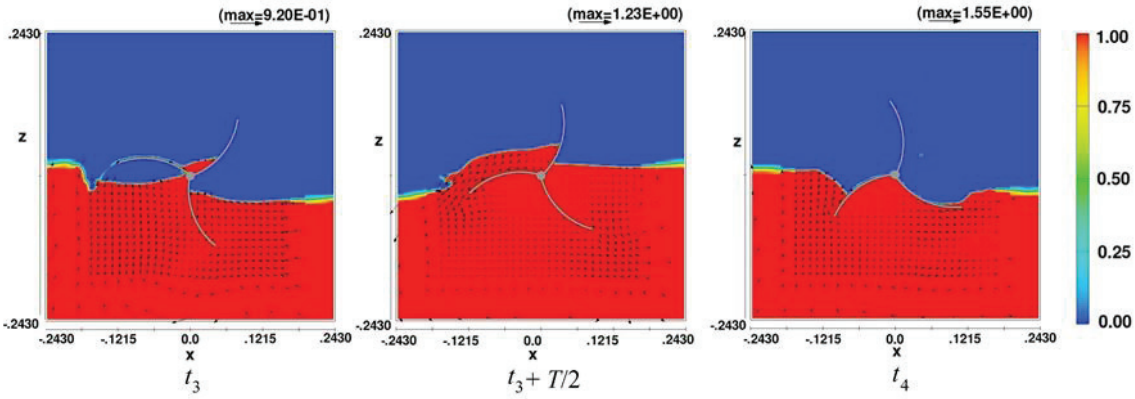

Fig. 5. Instantaneous phase contours and velocity vectors around the rotor over a one-wave period (*T)* between the end of the third wave cycle time (t_3) and of the fourth wave cycle time (t_4) at equal intervals at H = 100 mm, T = 1.5 s and z = 0 mm.

The different wave patterns are observed at different wave heights, periods and the submergence levels as shown in Figs. 6(a) to (g). These different phase contours and corresponding velocity vectors obtained for each case suggests that flow characteristics is strongly dependent upon differing wave propagation conditions and the energy

conversion rate may be increased with a proper combination of selected wave height. The submergence level of z = +50 mm clearly demonstrate ill-positioning of the rotor structure with very weak wave-rotor interactions leading to very low momentum exchange between the wave and the rotor, while maximum momentum exchange is observed for the case of H = 200 mm, T = 3.0 s , z = 0 mm. The intensity of the interaction of waves with the rotor device increases as the wave height increases and a combination of both streamwise and transverse wave motions is observed at higher wave heights.

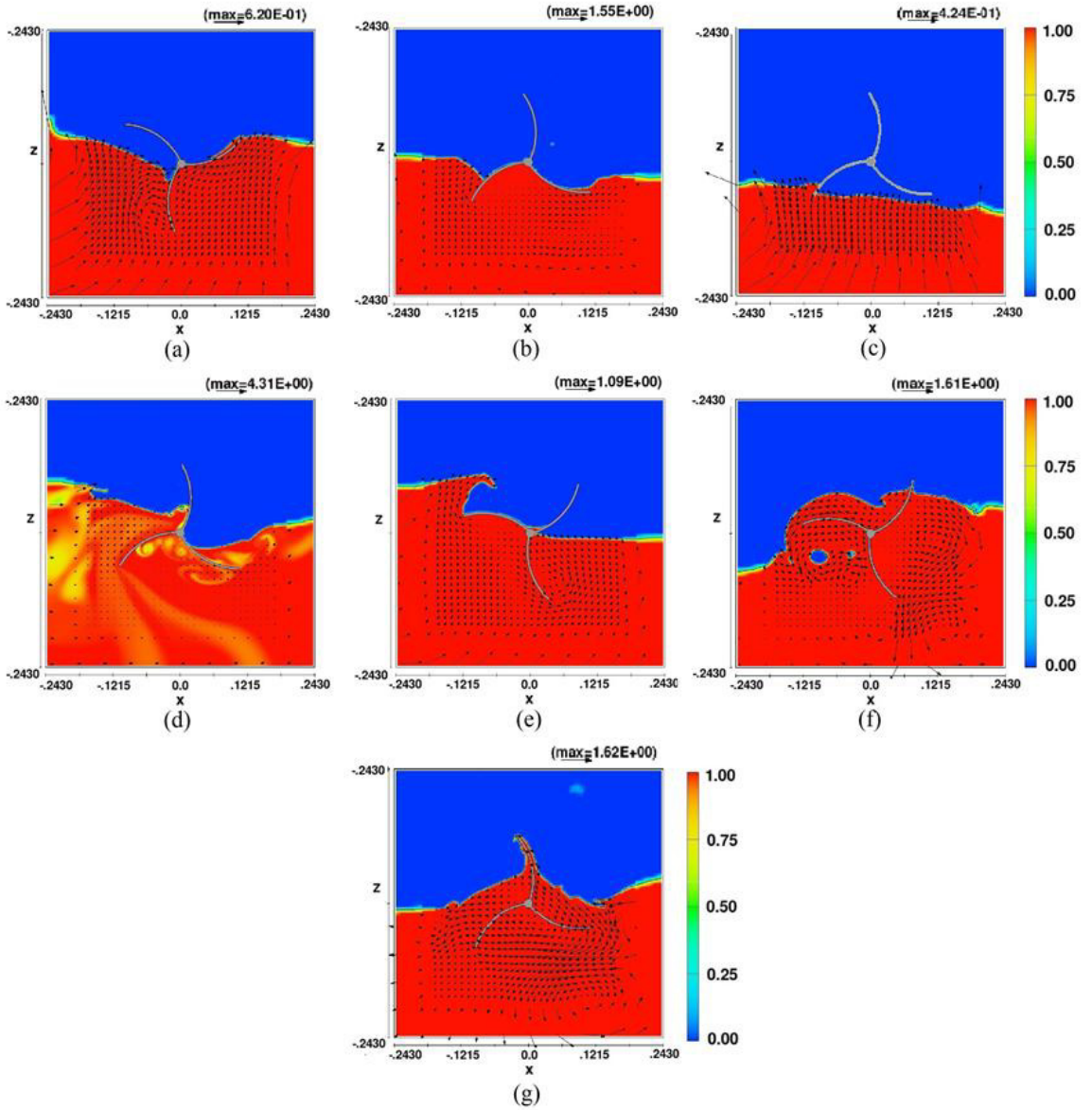

Fig. 6. Instantaneous phase contours and velocity vectors around the rotor at the end of the fourth wave cycle time (t_4); (a) H = 100 mm, T = 1.5 s , z = -50 mm; (b) H = 100 mm, T = 1.5 s , z = 0 mm; (c) H = 100 mm, T = 1.5 s , z = + 50 mm; (d) H = 150 mm, T = 1.5 s , z = 0 mm; (e) H = 200 mm, T = 1.5 s , z = 0 mm; (f) H = 200 mm, T = 3.0 s , z = 0 mm ; (g) H = 200 mm, T = 4.5 s , z = 0 mm

Further analysis is also accomplished for the rotational speed of the rotor at different wave parameters. The time history of the rotational speed for each wave period and wave height represents highly fluctuating rotational characteristics both in the clockwise and counter clock wise direction due to discontinuous fluid flow through the rotor blades and reproduces no steady and/or quasi steady rotational motion in the clock-wise direction due to a very low inertia of the Savonius rotor as illustrated in Figs 7(a) and (b). The higher fluctuating component obtained for higher values of wave height and/or wave period clearly signifies the effects of the wave height and/or wave period on the evolution of the rotational speed. From the figure, it is clearly identified that the effect of wave height and wave period on the history of the rotational speed of the rotor is more significant compared to that of submergence level for the selected submergence positions.

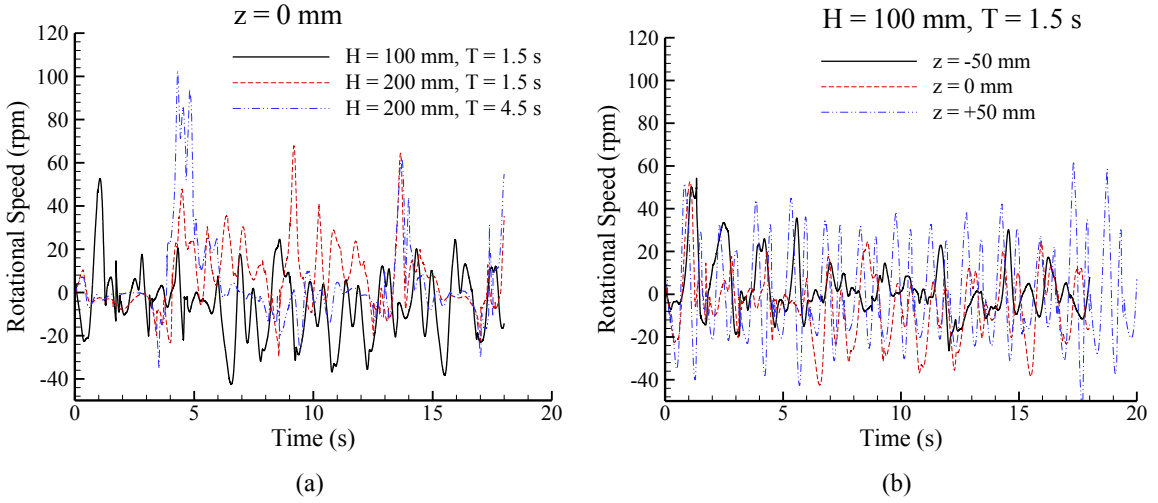

Fig. 7. The time history of the rotational speed recorded at different wave period and the wave height with varying submergence levels; (a) The recorded values at z = 0 mm; (b) The recorded values at H =100 mm and T = 1.5 s for different submergence levels.

Nevertheless, the average rotational speed, which is computed as the root mean square of the rotational speed values for all the corresponding data collected during each simulation interval, is found to be in the clockwise direction for each case, and shows a good correspondence with the experimental data as shown in Figs. 8(a) to (c). The increase in the wave height and/or wave period leads to higher average rotational speed regardless of which submergence level is adjusted.

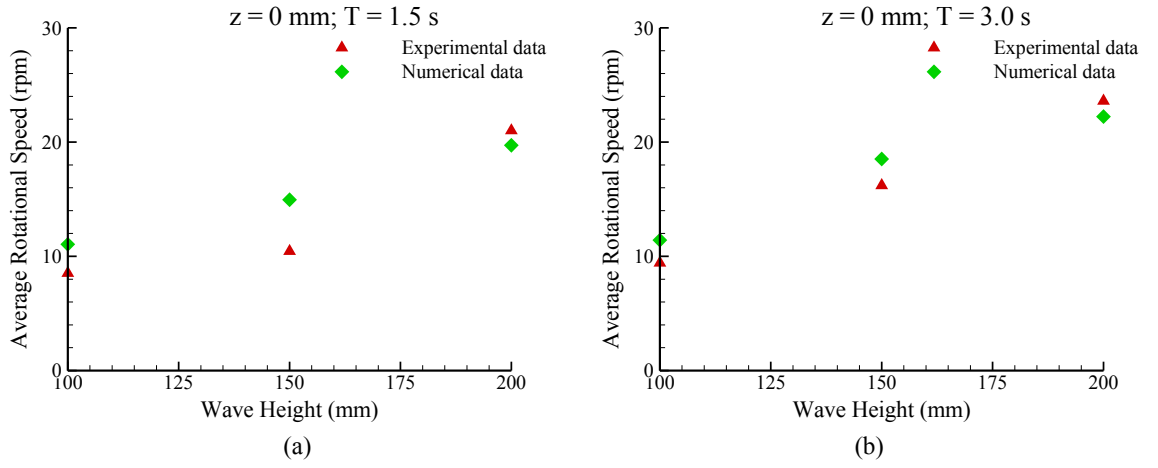

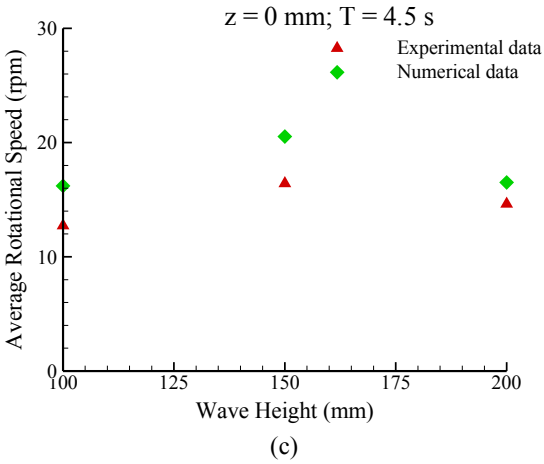

Fig. 8. The comparison of the numerical results of the effective rotational speed with the experimental data for different wave periods and the wave heights at a submergence level of $z = 0$ mm; (a) $T = 1.5$ s; (b) $T = 3.0$ s; (c) $T = 4.5$ s

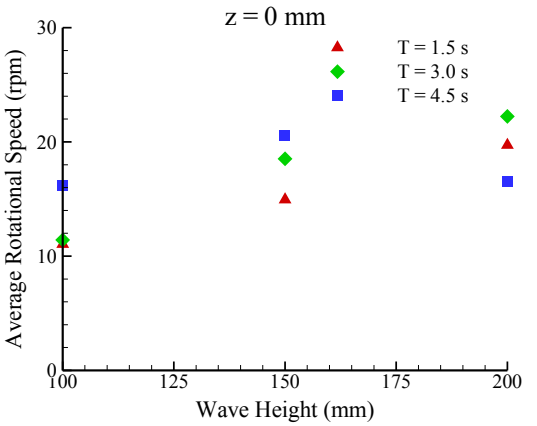

Fig. 9. The variation of the computed effective rotational speed in rotational per minute with the wave period and the wave height at a submergence level of $z = 0$ mm

It is noted here that higher angular momentum transfer towards the rotor blade is achieved when the rotor is just placed on water surface level i.e. submergence level of $z = 0$ mm, and the computed effective rotational speed values computed at this surface level are compared with each other at different wave height and wave periods as shown in Fig. 9. As seen from the figure, the higher the wave period and/or wave height the higher the effective rotational speed in general. When the wave height is increased from $H = 150$ mm to $H = 200$ mm, at higher wave period of $T = 4.5$ s, the effective rotational speed decreases due to discontinuous and/or wave breaking effects as previously observed in the experimental study [5].

4. Conclusions

The regular surfaces waves based on Stokes 2nd wave theory are successfully reproduced computationally in a numerical wave flume (NWF) which is representative of the experimental wave flume (EWF) used in the previous experimental study of the authors. The wave-rotor interactions for the horizontally places 3-bladed Savonuius rotor

device are later studied computationally for different wave heights, wave period and submergence level in the intermediate water depth to comparatively examine the optimum wave and submergence positioning for the investigated wave propagation range. The computed effective rotational speed results demonstrate a good correspondence with the corresponding determined values of the previous experimental data. The higher rotational speed is obtained for the submergence positioning of $z = 0$ mm, at higher wave height and wave periods as an indication of more profound effects of the wave period and wave height compared to submergence level. The positive submergence has negative effect on the momentum exchange between the wave and the rotor, and hence low values of the rotational speeds are obtained at positive submergence level. The overall results also signify that the present numerical approach could be a reliable tool for further studying such phenomena for the future applications.

Acknowledgements

This work was partially funded by the Basque Government under the project of the Gobierno Vasco- Basica y Aplicada - PI 2011-8.

References

[1] Hindasageri V, Ramesh H, Kattimani SC. Performance of Savonious rotors for utilizing the orbital motion of ocean waves in shallow waters. Journal of Sustainable Energy & Environment 2011; 2:117-119
[2] Faizal M, Ahmed MR, Lee YH. On utilizing the orbital motion in water waves to drive a Savonius rotor. Renewable Energy 2010; 35:164–169
[3] Nakajima M, Shouichiro, I, Ikeda T. Performance of double-step Savonius rotor for environmentally friendly hydraulic turbine. Journal of Fluid Science and Technology 2008; 3(3): 410-419
[4] Tutar, M, Veci, I. Experimental study on performance assessment of Savonius rotor type wave energy converter in an experimental wave flume. IET Renewable Power Energy 2016; 10(4): 541-550
[5] Tutar, M, Veci I. Performance analysis of a horizontal axis 3-bladed Savonius type wave turbine in an experimental wave flume (EWF)- Renewable Energy 2016;86 : 8-25
[6] Ahmed MR, Faizal M, Prasad K, Cho, YJ, Kim CG, Lee, YH. Exploiting the orbital motion of water particles for energy extraction from waves. Journal of Mechanical Science and Technology 2010; 24 (4): 943-949
[7] Zullah MA, Lee YH. Performance evaluation of a direct drive wave energy converter using CFD. Renewable Energy 2012; 49: 237-241
[8] Tutar M., Erdem, C., A Study of Energy Conversion Efficiency of a Savonius Type Energy Converter System. In: Proc. of International Conference on Energy Efficiency and Energy Related Materials (ENEFM2013), Oct. 9-12 2013, Kemer, Antalya, Turkey.
[9] Tutar M, Erdem, C. Computational modelling of two-phase flow around a Savonius type wave energy converter in a two-dimensional numerical wave tank. In: Proc. of The 5th International Conference on Computational Methods in Marine Engineering (MARINE 2013), May 29-31 2013, Hamburg, Germany
[10] Yakhot V, Orszag SO. Renormalization group methods in turbulence. Journal of Scientific Computing 1986; 1(1): 1–51.
[11] Hirt CW, Nichols, BD. Volume of fluid (VOF) method for the dynamics of free boundaries. J. Computational Phys. 1981; 39(1): 201–225.
[12] FLOW3D, V10.0.2.05, Flow Science Inc. Santa Fe, NM, USA, 2012
[13] Wei G. A fixed-mesh method for general moving objects in fluid flow. International Journal of Modern Physics B 2005; 19 (28-29): 1719-1722.